First publ. in: Physical Review B 75 (2007), 144428

Micromagnetism and magnetotransport properties of micron-sized epitaxial $CrO_2(100)$ wires

C. König,[1] M. Fonin,[2] M. Laufenberg,[2] A. Biehler,[2] W. Bührer,[2] M. Kläui,[2] U. Rüdiger,[2] and G. Güntherodt[1]
[1]*II. Physikalisches Institut, Rheinisch-Westfälische Technische Hochschule Aachen, 52056 Aachen, Germany*
[2]*Fachbereich Physik, Universität Konstanz, 78457 Konstanz, Germany*

We report a detailed study of the magnetic domain configurations and the magnetization reversal in epitaxial $CrO_2(100)$ wires (0.5–5 μm widths) patterned along different crystallographic directions. Magnetic force microscopy imaging in zero field reveals single domain states for wires fabricated along the magnetic easy axis, while wires perpendicular to the magnetic easy axis exhibit a stripe domain configuration. The behavior in an applied field and the switching of the magnetization is probed by magnetoresistance (MR) measurements. Depending on the orientation of the wire with respect to the easy and hard magnetocrystalline anisotropy axes and the field direction, distinctly different reversal modes are observed including inhomogeneous magnetization configurations. These modes and configurations can be explained taking into account the interplay between the different anisotropy terms. MR measurements at variable temperatures demonstrate that the low temperature MR response is dominated by intergrain-tunneling magnetoresistance, while at elevated temperatures it is superseded by the anisotropic MR.

PACS number(s): 75.47.−m, 85.70.Kh, 72.80.Ga

I. INTRODUCTION

Since the discovery of the giant magnetoresistance (GMR) effect in 1988[1,2] spin-dependent transport effects in magnetic layers have become one of the major areas of basic research and technology. In recent years, a number of devices have been developed where both the charge and spin of electrons are exploited using spin-dependent transport, such as magnetic random access memory cells.[3–5] The performance of such spintronic devices can be enhanced using ferromagnetic materials exhibiting a high degree of spin polarization. Of particular interest are so-called "half-metallic ferromagnets," compounds that are metallic for one spin component while insulating for the other spin component leading to 100% spin polarization at the Fermi energy (E_F). One of the most promising materials in this regard is chromium dioxide.

Chromium dioxide (CrO_2) is a metallic ferromagnetic oxide (T_C=393 K)[6] which has been widely used as a recording medium in magnetic tapes. CrO_2 crystallizes in a tetragonal rutile structure with lattice parameters of $a=b=4.421$ Å and $c=2.916$ Å. The chromium ions are present in the Cr^{4+} state with a magnetic moment of 2 μ_B per ion. Band structure calculations predict CrO_2 to be a half-metallic ferromagnet with 100% spin polarization of the conduction electrons at E_F.[7–9] This prediction has been validated by several experimental observations, such as point contact Andreev reflection,[10–12] the Tedrow-Meservey spin-polarized tunneling technique,[13] and spin-resolved photoelectron spectroscopy measurements,[14,15] indicating a very high spin polarization up to 97% at 1.2 K[13] as well as above 90% at room temperature (RT).[15]

Epitaxial $CrO_2(100)$ thin films grown on $TiO_2(100)$ have an intrinsic magnetocrystalline anisotropy with a pronounced magnetic easy axis parallel to the in-plane [001] direction (c axis). The experimental observations concerning the magnetic anisotropy of CrO_2 (Refs. 6, 16, and 17) have been theoretically confirmed by local spin density approximation calculations[18] where the [001] direction of $CrO_2(100)$ films has been identified as the magnetic easy axis and the [010] direction as the magnetic hard axis. The corresponding uniaxial anisotropy constant K_1 has been determined by several groups to be 19,[19] 27,[20] or 44 kJ/m^3 (Ref. 6) depending on the structural quality of the films as well as on the film thickness. However, along with the magnetocrystalline anisotropy the strain anisotropy has to be considered in order to explain the magnetic properties of the CrO_2 films.[6,21] The strain resulting from the lattice mismatch between $CrO_2(100)$ and $TiO_2(100)$ substrate was found to have a strong influence on the magnetic anisotropy of CrO_2 films. Miao *et al.*[21] reported the reorientation of the magnetic easy axis upon variation of the CrO_2 film thickness, switching from the in-plane [001] direction for films thicker than 250 nm to the [010] direction for thinner films (<50 nm). This unusual behavior results from the inhomogeneous distribution of the strain in thin CrO_2 films.[21]

Magnetoresistance (MR) measurements have been reported on compact powders,[22,23] polycrystalline films,[17,24–28] as well as single crystalline films of CrO_2.[17,29–31] Hysteretic MR was observed on powder compacts with an MR ratio of about 40% at 4.2 K.[23] The MR was reported to decrease rapidly with increasing temperature to less than 1% at RT.[22,23] The large MR effect observed in the compacted powders of CrO_2 is attributed to the low-temperature tunneling of spin-polarized electrons across grain boundaries which is superseded by electron hopping without spin conservation at higher temperatures. By diluting a ferromagnetic CrO_2 with insulating antiferromagnetic Cr_2O_3 powder, a reduction of the conductivity by three orders of magnitude was observed accompanied by a substantial enhancement of MR from 29% to 50% at 5 K supporting the intergrain tunneling mechanism.[22]

Similar behavior was also reported for polycrystalline CrO_2 films prepared by high-pressure thermal decomposition of CrO_3 on $SrTiO_3$,[24] as well as Al_2O_3 and TiO_2 substrates.[25] Hwang and Cheong[24] observed a negative MR of about 10%

at 5 K and 2 T for the as-prepared CrO_2 samples. Subsequent high-temperature postannealing of the samples resulted in an increase of the resistivity by about three orders of magnitude at low temperatures and an enhancement of the MR to about 24% at 5 K. The increase of MR in the postannealed films was attributed to the modification of the effective intergrain tunneling barrier due to the decomposition of CrO_2 into insulating Cr_2O_3 at the grain surface.

Gupta *et al.*[17] studied the high-field and low-field MR properties of the epitaxial $CrO_2(100)$ films grown on $TiO_2(100)$ substrates and observed positive 25% MR at 5 K and 4 T in transverse geometry ($I \perp H$) with current parallel to the [001] direction. The positive MR observed at low temperatures was attributed to the Lorentz force effect, which can be related to the mean free path and further to the crystalline properties of the films.[32,33] More recently, a detailed MR study of epitaxial $CrO_2(100)$ films was performed between 4.2 and 300 K in magnetic fields up to 23 T reporting three characteristic MR regimes.[30,31] At low magnetic field (<0.1 T) and at low temperatures (4.2 K), intergrain tunneling MR (ITMR) dominates, whereas in the high-field regime ordinary Lorentz force MR is reported to be the dominant contribution to the MR. In the intermediate-field range, spin-dependent scattering at weakly bound spins in the vicinity of grain boundaries seems to be the leading source of negative MR contribution showing a linear increase with increasing temperature. The observed linear and negative MR at high temperatures was interpreted in terms of a double-exchange mechanism of CrO_2. The magnitude of the anisotropic MR (AMR) was reported to be less than 0.1% over the whole temperature range investigated.

So far, studies have concentrated on the properties of CrO_2 continuous films and in particular, the MR investigations have focused on continuous films or macroscopic (>100 μm) elements. On the other hand, both for applications and for understanding fundamental physical effects related to the high spin polarization, such as domain wall magnetoresistance effects and current-induced domain wall propagation,[34–36] controlled magnetization configurations and reversal processes have to be obtained. This is only possible in magnetic micro- or nanostructures, where the physical properties can be tailored by engineering the geometry. The most widely used geometry is a wire, where simple and reproducible domain structures are attained and which might also prove useful for applications such as in the racetrack memory device.[37] In order to use CrO_2 wires, a detailed understanding of the magnetization states as well as reversal processes that result from the interplay of the shape and the intrinsic magnetocrystalline anisotropy has to be obtained.

In this paper we report on a detailed study of the magnetic properties of microstuctured epitaxial CrO_2 wires of different widths and oriented along different crystallographic directions. The remanent magnetization configurations for the different geometries at zero field have been determined by means of magnetic force microscopy (MFM) measurements. In order to probe the magnetic switching behavior in an applied field, MR measurements were carried out. Magnetotransport at variable temperatures has revealed that the MR response of the wires is dominated by AMR and ITMR, respectively, at high and low temperatures. Detailed measurements for the different wire geometries have revealed intricate reversal mechanisms that strongly depend on the directions of the external magnetic field with respect to the wire long axis as well as the magnetocrystalline axes. These reversal mechanisms result from the interplay of the wire geometry with respect to the magnetocrystalline anisotropy and the Zeeman energy of the magnetic moments due to the applied field.

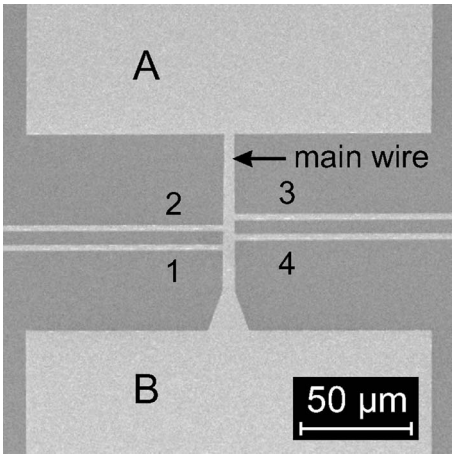

FIG. 1. SEM image of a CrO_2 transport structure consisting of the main wire connected to two contact pads (A and B) and four additional contact leads (1–4) with contact pads (not shown).

II. EXPERIMENT

Epitaxial $CrO_2(100)$ films were grown on single crystal $TiO_2(100)$ substrates by chemical vapor deposition (CVD) using CrO_3 as a precursor. The source temperature was kept at 270° within a quartz tube in a one-zone furnace. A heating cartridge implemented in the substrate holder was used to achieve 390–410 °C at the TiO_2 substrate to promote CrO_3 decomposition. The sublimed CrO_3 precursor is transported by an O_2 carrier gas flow (1 atm, 10 cc/min) from the source region to the substrate in the reaction zone where it decomposes to form CrO_2. Prior to deposition the TiO_2 substrates were cleaned in organic solvents (acetone, isopropanol, and methanol) and subsequently etched in an HF aqueous solution. The typical thickness of the prepared $CrO_2(100)$ films was estimated to be about 60 nm. The described preparation technique was confirmed to yield single-phase epitaxial $CrO_2(100)$ films (T_C=385 K) showing a high spin polarization at the Fermi energy at room temperature.[15,38]

Wires of different widths (0.5, 1, 2, and 5 μm) together with leads and contact pads were fabricated from epitaxial $CrO_2(100)$ films by conventional electron-beam lithography in conjunction with Ar^+ ion milling. Figure 1 shows a scanning electron microscopy (SEM) image of a typical CrO_2 microstructure consisting of the main wire (vertical line) with two main contact pads (bottom and top), and four additional contact leads (horizontal lines) connected to four contact pads (not shown). In order to ensure reproducible magnetization reversal processes, one end of the main wire was

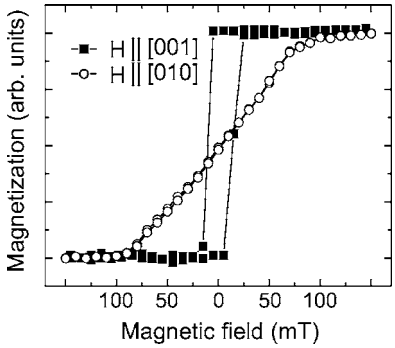

FIG. 2. MOKE hysteresis loops of a $CrO_2(100)$ film with the magnetic field applied along the [001] direction (magnetic easy axis) and along the [010] direction (magnetic hard axis).

always patterned asymmetrically (lower part of the main stripe). This asymmetrically patterned end of the CrO_2 wire acts as a nucleation pad for the domain walls which always nucleate at this end. In Fig. 1 the main wire is aligned parallel to the [001] direction, i.e., magnetic easy axis, of the $CrO_2(100)$ film. In the following these structures will be referred to as *easy structures* whereas the microstructures with the main wires aligned perpendicular to the [001] direction will be referred to as *hard structures*.

Atomic force microscopy (AFM) as well as MFM measurements on the CrO_2 wires were performed at room temperature by using a Digital Instruments MULTIMODE™ scanning probe microscope. Cobalt coated low moment POINTPROBE-PLUS® Silicon-SPM-Sensors from Nanosensors™ were used as cantilevers in all MFM experiments.

The MR measurements were carried out in a temperature range from 4.2 to 300 K in a liquid ^{4}He bath cryostat setup. Two vector coils in a perpendicular arrangement yield maximum magnetic fields of 515 mT and 140 mT giving the possibility of applying an external magnetic field in any in-plane direction of the sample. A standard lock-in technique was used to measure the resistance in a four point configuration.

III. RESULTS AND DISCUSSION

Prior to microstructuring and the MR measurements the magnetic properties of the $CrO_2(100)$ films were investigated by means of magneto-optical Kerr effect (MOKE) at room temperature. Figure 2 shows typical MOKE hysteresis loops of the $CrO_2(100)$ film with the magnetic field applied along the [001] direction (closed squares) as well as along the [010] direction (open circles). The prepared $CrO_2(100)$ films exhibit an intrinsic uniaxial in-plane anisotropy with a pronounced magnetic easy axis parallel to the [001] direction. The magnetocrystalline anisotropy constant K_1 is given by $1/2(H_K M_S)$ where M_S is the saturation magnetization and H_K is the anisotropy field.

From the magnetization data along the in-plane [010] direction the anisotropy field H_K=90 mT was determined. Considering the saturation magnetization of 655 emu/cm^3 determined by superconducting quantum interference device magnetometery, the anisotropy constant K_1 was calculated to

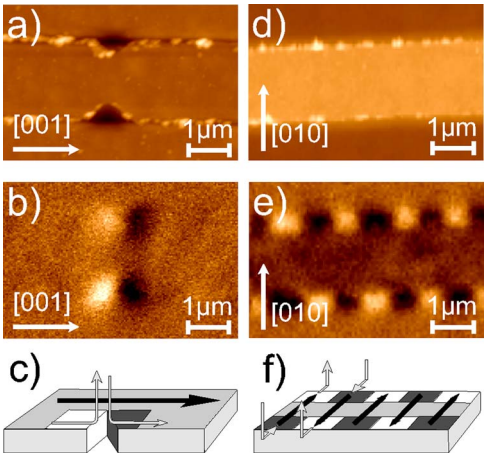

FIG. 3. (Color online) AFM [(a) and (d)] and MFM images [(b) and (e)] of 2 μm wide CrO_2 wires fabricated along the [001] direction [(a) and (b)] and the [010] direction [(d) and (e)]. Schematics (c) and (f) represent the MFM contrast formation due to the stray fields for both configurations.

be 29 kJ/m^3, which is in good agreement with the value of K_1=27 kJ/m^3 measured by Yang *et al.* on epitaxial CrO_2 films.[20]

Figure 3 shows AFM [(a) and (d)] and MFM [(b) and (e)] images of the 2 μm wide CrO_2 wires fabricated parallel (*easy structure*) as well as perpendicular (*hard structure*) to the [001] in-plane crystallographic direction of the film. Prior to the MFM imaging, the *easy structure* was magnetized in the field applied parallel to the [001] direction of the CrO_2 film whereas the *hard structure* was demagnetized in an alternating magnetic field with a decreasing amplitude. The *easy structure* is in a single domain remanent state showing MFM contrast only at the artificially introduced constriction [Fig. 3(b)]. The schematic in Fig. 3(c) illustrates the formation of the MFM contrast due to the magnetic stray fields (white lines and arrows) at the constriction with the in-plane magnetization (black arrow) aligned along the wire. The remanent magnetic state of the *hard structure* exhibits a stripe domain pattern visible due to the alternating stray field contrast at the wire edges in the MFM image [Fig. 3(e)]. The magnetization within the alternating, approximately 500 nm wide domains, lies parallel to the easy axis which is shown in the schematic [Fig. 3(f)]. In this case, a shape anisotropy with the easy axis parallel to the long axis of the wire and perpendicular to the magnetocrystalline easy axis leads to a stripe domain configuration which minimizes the free energy.[39,40]

In order to identify the MR response of the CrO_2 wires, so-called rotational scans were measured as shown in Fig. 4. The measurements were performed on the *easy structure* [(a) and (b)] as well as on the *hard structure* [(c) and (d)] at 4.2 K (left-hand panels) and 190 K (right-hand panels). By taking rotational scans the electrical resistance was measured as a function of the angle between the applied magnetic field and the direction of the current given by the orientation of the CrO_2 wire. The amplitude of the magnetic field has been 125 mT in all orientations. The direction of the field is defined as 0° (or 180°) and 90° (or 270°) if it is applied parallel

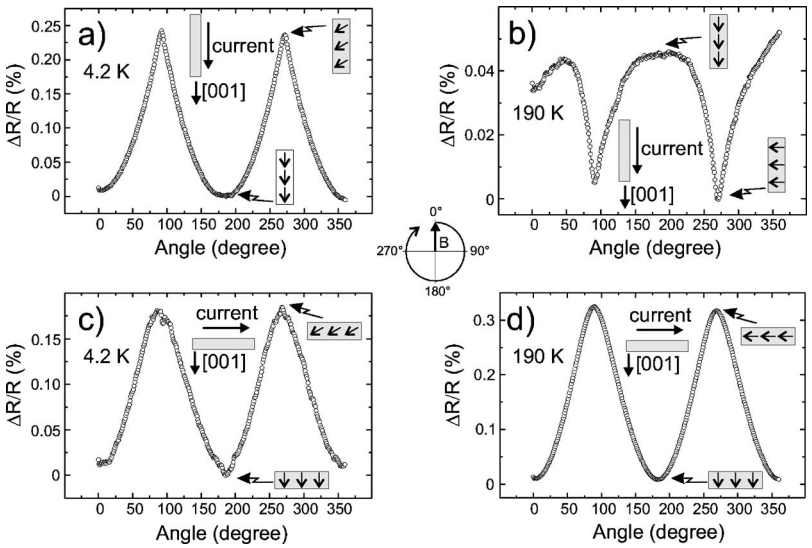

FIG. 4. Rotational scans measured on the 2 μm wide *easy structure* [(a) and (b)] as well on the 2 μm wide *hard structure* [(c) and (d)] at 4.2 K (left-hand panels) and at 190 K (right-hand panels). The direction of the magnetic field (see inset in the center) is defined as 0° (or 180°) and 90° (or 270°), respectively, if it is applied parallel and perpendicular to the [001] direction, i.e., the magnetic easy axis, of the CrO_2 film. In all plots the orientation of the magnetization of the CrO_2 grains is shown for minimum and maximum resistance.

and perpendicular to the [001] direction of the CrO_2 film, respectively. Figure 4(a) shows a rotational scan performed on the *easy structure* with a 2 μm wide CrO_2 wire. The resistance shows minima at 0° and 180°, i.e., when the external field is parallel to the magnetic easy axis, which can be understood in terms of low-field ITMR effect. In this case both the magnetic field and the magnetocrystalline anisotropy of CrO_2 lead to the parallel alignment of the magnetization of the CrO_2 grains reducing the electron scattering at the grain boundaries resulting in a resistance minimum. With a magnetic field applied perpendicular to the [001] direction of CrO_2 (90° and 270°) the resistance reaches its maximum. Here, the magnetization of the neighboring grains is slightly tilted with respect to each other due to the fact that the external field acts in the direction perpendicular to the magnetic easy axis direction yielding a lowering of the tunneling probability across a grain boundary and leading as a consequence to a higher resistance. Figure 4(b) shows a rotational scan of the same *easy structure* taken at 190 K. The MR curve is not periodic over 360° due to the thermal drift during the resistance measurement. The MR behavior is inverted compared to the measurements at 4.2 K showing the resistance maxima at 0° and 180°. Here [Fig. 4(b)] the AMR effect supersedes the ITMR effect and causes a minimum of resistance (90° and 270°) when the magnetic field is applied perpendicular to the current direction (here the [001] direction), whereas the parallel orientation of the current and the magnetization results in the maximum resistance values (0° and 180°). Low temperature measurements on the *hard structure* [Fig. 4(c)] show that the resistance extremal points are at the same positions as in the case of the *easy structure* [Fig. 4(a)], although the wire long axis as well as current have been rotated by 90°. However, at higher temperature (190 K) the inverting of the resistance curve was not observed [Fig. 4(d)] as in the *easy structure* [Fig. 4(b)]. Here both ITMR and AMR effects cause a minimum of the resistance at 0° and 180°. Furthermore, these rotational scans demonstrate the influence of the shape anisotropy on the magnetization process: the maxima of the resistance curve in Fig. 4(a) at 90° and 270° are very sharp, whereas the minimum at 180° is broadened. This can be attributed to the fact that a 90° or 270° orientation of the magnetization of the *easy structure* is energetically unfavorable with respect to both magnetocrystalline and shape anisotropy. In the case of the *hard structures* [Fig. 4(c)] the magnetization orientations at the minima and maxima of resistance are energetically unfavorable as here the anisotropy contributions are aligned perpendicular to each other. Further rotational scans at various temperatures showed that the transition from the regime dominated by the ITMR effect to the AMR dominated regime lies between 80 and 120 K. These results show that all magnetoresistive effects presented in the following measurements at 4.2 K are due to the ITMR effect and all possible contributions of the AMR effect can be neglected.

In order to investigate the interplay between different anisotropy contributions in CrO_2 wires, magnetization reversal processes of both *easy* and *hard structures* were studied by MR measurements for different magnetic field orientations. Figure 5 shows the MR as a function of magnetic field for the 2 μm wide *easy structure* with the magnetic field applied parallel (a) and perpendicular (b) to the [001] direction measured at 4.2 K. The magnetization reversal process of the *easy structure* with $\vec{B}\|[001]$ [Fig. 5(a)] is characterized by a slow increase of resistance (points 1–3) followed by a sharp resistance drop at about 28 mT (point 4) and a subsequent slow decrease (point 5). At high fields (point 1) the magnetic field as well as shape and magnetocrystalline anisotropy align the magnetization of the neighboring grains parallel to each other which results in a resistance minimum. With the decreasing magnetic field the misalignment of the local magnetization of neighboring grains increases which is due to the initial slight variation of the easy magnetic axis direction of individual grains. After crossing zero field, the parallel alignment of the magnetization of the adjacent grains is further distorted because the magnetic field is now applied antiparallel to the magnetization direction of the grains. The MR drop at about 28 mT (point 3) is attributed to the magnetization reversal process, i.e., domain wall formation at the contact wide pads followed by the domain wall propagation along the wire. By increasing the magnetic field the magnetic moments of the single grains are being aligned along the field resulting in a resistance decrease (point 5).

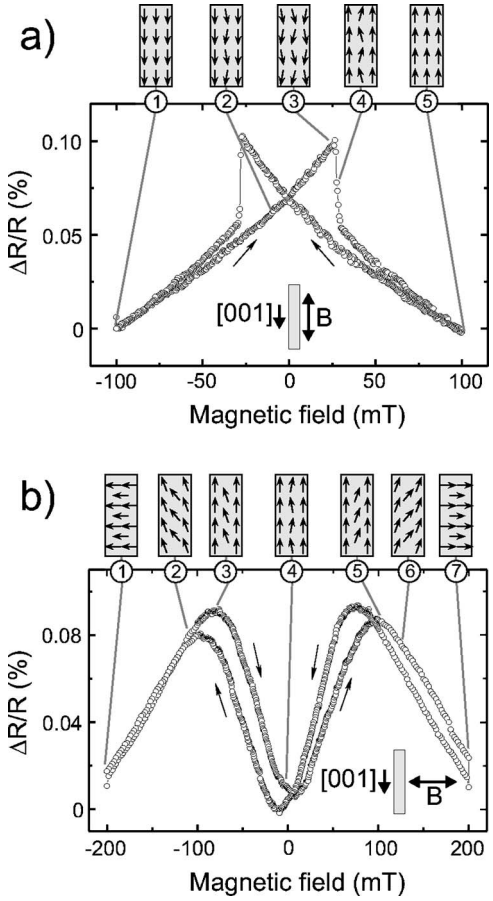

FIG. 5. The field dependence of the MR of the 2 μm wide *easy structure* with the magnetic field applied parallel (a) and perpendicular (b) to the [001] direction measured at 4.2 K. Schematics at the upper side of each plot represent different magnetization configurations during the magnetization reversal process.

The MR curve measured at the same 2 μm wide *easy structure* with $\vec{B} \perp [001]$ is shown in Fig. 5(b). In this case MR increases with decreasing magnetic field (points 1–3) reaching the maximum value at about −75 mT (point 3) and decreasing subsequently to the minimum at zero field (point 4). Exactly the same MR behavior is observed by increasing magnetic field from 0 to 200 mT which is due to the symmetry of the experiment. The initial increase of the resistance (points 1–3) can be explained by the magnetization misalignment of neighboring grains resulting from the rotation of the local magnetization starting from the edge to the center of the wire. At the edge both shape and magnetocrystalline anisotropy tend to align the local magnetization parallel to the [001] (parallel to the wire axis) whereas the contribution of the shape anisotropy in the center of the wire is lower leading to the rotation of the local magnetization further towards the field. The resistance maximum (point 3) is achieved when the rotation angle between the spins at the edge and in the center is maximized. With decreasing magnetic field, shape and magnetocrystalline anisotropy lead to the alignment of the magnetization parallel to the [001] direction. By reducing the magnetic field to 0 T the magnetization of the neighboring grains within the wire is aligned parallel to the

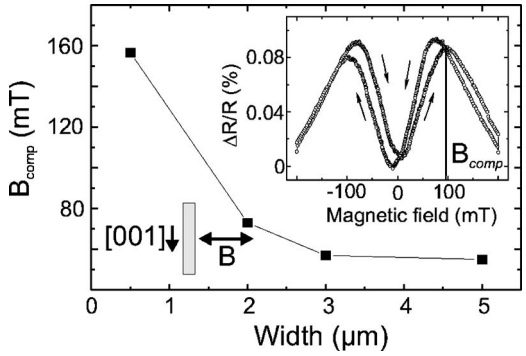

FIG. 6. The compensation field (B_{comp}), i.e., the position of the MR maxima, is shown as a function of the CrO_2 wire width. The inset shows the MR ratio of a CrO_2 *easy structure* as a function of external magnetic field which is applied perpendicular to the [001] direction of CrO_2. The position of the MR maximum is marked as B_{comp}.

[001] direction, i.e., along the CrO_2 wire with resistance reaching a local minimum at zero field (point 4). This model is supported by the fact that the position of the MR maxima shifts to the higher magnetic field with the decreasing width of the CrO_2 wire. Figure 6 shows the compensation field B_{comp}, i.e., the position of the maxima (points 3 and 5), as a function of the CrO_2 wire width. With a decreasing width of the wire a higher magnetic field is needed to overcome the shape anisotropy contribution. For widths larger than 3 μm the influence of the shape anisotropy on B_{comp} vanishes, so that the magnetization reversal process in this regime is mainly dominated by the magnetocrystalline anisotropy.

The magnetization reversal process of the *easy structures* is drastically different from that of the *hard structures* where the long axis of the CrO_2 wire is perpendicular to the [001] direction, i.e., the magnetic easy axis, and here the shape and magnetocrystalline anisotropy compete against each other. Figure 7(a) shows the MR as a function of magnetic field for the 2 μm wide *hard structure* measured at 4.2 K with $\vec{B} \| [001]$. The magnetization reversal process is characterized by a slow increase of the resistance (points 1–3) followed by a resistance drop at about 27 mT (points 3 and 4) and a subsequent slow decrease (points 4 and 5). Here the increase of the resistance (points 1 and 2) can be again attributed to the magnetization misorientation of the neighboring grains in a decreasing magnetic field. Close to zero field this process is supported by the nucleation and propagation of domain walls and leading as a consequence to the formation of the stripe domain structure which was observed in the MFM measurements [Fig. 3(e)]. However, the domain walls between the stripe domains only have a small influence on the resistance, as no jumps in the MR curve were observed that allow identification of single domain wall nucleation. Thus here ITMR is at the origin of the MR and intrinsic domain wall effects are smaller. Increasing the external magnetic field (points 2 and 3) leads to a stronger local magnetization alignment in the domains with the magnetization parallel to the field which is superseded by the simultaneous magnetization misalignment of the neighboring grains in the domains with the magnetization antiparallel to the applied magnetic field lead-

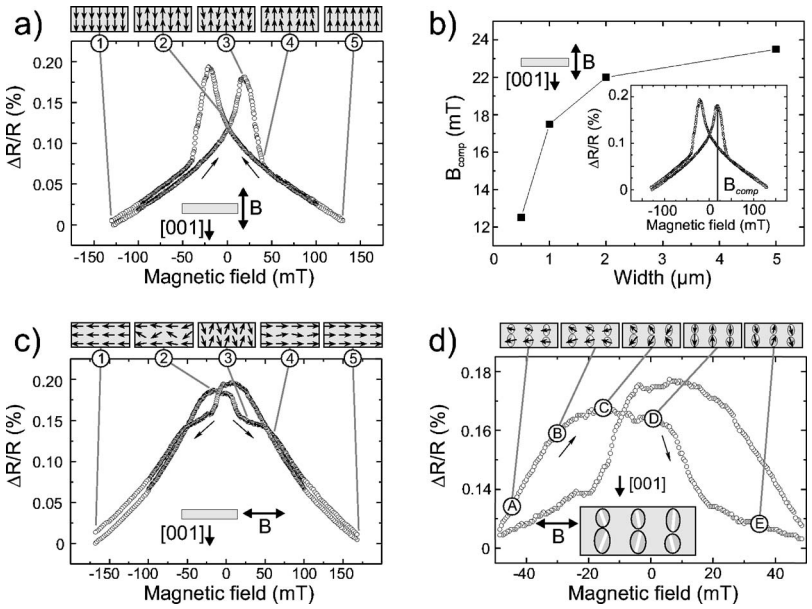

FIG. 7. (a) The field dependence of the MR of the 2 μm wide *hard structure* measured at 4.2 K with the magnetic field applied parallel to the [001] direction. In (b) the compensation field (B_{comp}) as a function of the CrO_2 wire width is presented. The inset shows the MR of a CrO_2 *hard structure* as a function of external magnetic field which is applied parallel to the [001] direction with the position of the MR maximum marked as B_{comp}. (c) The field dependence of the MR ratio of the 2 μm wide CrO_2 *hard structure* with the magnetic field applied perpendicular to the [001] direction. (d) A zoom-in on the field dependence of the MR ratio of the same 2 μm wide *hard structure* with the magnetic field applied perpendicular to the [001] direction of CrO_2. Schematics at the upper side of the plots (a), (c), and (d) represent different magnetization configurations during the magnetization reversal process.

ing to a higher resistance reaching its maximum at point 3. The further increase of the external field (points 3 and 4) leads to the formation of a monodomain state with the magnetization parallel to the external field, i.e., perpendicular to the long axis of the wire. The continuous growth of the stripe domains which are parallel to the external field decreases the resistance. This process finishes at point 4 and the further slow decrease of the resistance is due to the stronger parallel alignment of the magnetization of neighboring grains. The formation of stripe domains with alternating magnetization is energetically more favorable in narrower wires due to a stronger shape anisotropy contribution which allows easier nucleation of reverse domains. This is corroborated in the corresponding MR measurements on wires of different widths [Fig. 7(b)]. In the CrO_2 wires of smaller width the transition from the stripe domain state to the monodomain state occurs at lower fields (B_{comp}).

Figure 7(c) shows the magnetization reversal process of a 2 μm wide *hard structure* at 4.2 K with $\vec{B} \perp [001]$, i.e., parallel to the main wire axis. Here, the resistance increases to the maximum at about zero field (points 1 and 2) followed by a small decrease (points 2 and 3) with a plateau (point 3) and a further decrease (points 4 and 5). At high negative fields (point 1) the magnetization is aligned along the wire but perpendicular to the magnetic easy axis showing the minimum of the resistance. Upon decreasing of the external field the magnetization misorientation of the neighboring grains due to the magnetocrystalline anisotropy leads to the resistance increase (points 1 and 2). This effect is smaller at the edge of the wire due to the shape anisotropy contribution aligning the magnetization in the direction parallel to the wire. With further decreasing external field the magnetization rotation continues and is followed by the formation of stripe domains which are, however, tilted to the field direction accompanied by the formation of the head-to-head and tail-to-tail domain walls close to the center of the wire. The formation of the head-to-head as well as tail-to-tail domain walls can be explained by a slightly different orientation of the magnetic easy axis in different grains forcing a formation of domains tilted to each other. In Fig. 7(d) a zoom into the center part of the resistance curve at about zero field is presented. As described above the presence of the MR maximum (points A, B, and C) can be explained by considering different crystallites of the CrO_2 film [see the schematic in the lower part of Fig. 7(d)]. Each crystallite exhibits a magnetic easy axis, the direction of which differs slightly from that of the macroscopic easy axis of the CrO_2 film. These different easy axes are marked by the white lines in the schematic in Fig. 7(d). The transition from the monodomain state into the stripe domain state starts with the rotation of the magnetization of the crystallites towards their corresponding magnetic easy axes (points A, B, and C). This reversible process is followed by an irreversible switching of the magnetization into the stripe domain state (point D). During this switching process due to the exchange coupling, first the magnetizations of the smaller grains align with those of the adjacent larger grains to form domains. By the formation of a nearly perfect stripe domain pattern the resistance goes down (after point D). At the point E the external magnetic field is high enough to rotate the magnetization of the grains out of the stripe domain pattern. Increasing the external field leads to the transition from the stripe domain state to the monodomain state with the magnetization parallel to the main wire axis accompanied by a resistance decrease (points 3 and 4). Further resistance decrease (points 4 and 5) is again due to the stronger parallel alignment of the magnetization of neighboring grains.

In order to show that the magnetization reversal process becomes irreversible at about 0 mT [point D in Fig. 7(d)] minor hysteresis loops were measured on the same 2 μm wide *hard structure* ($\vec{B} \perp [001]$) which are shown in Fig. 8. The minor hysteresis loops were measured in dependence on the amplitude of the applied magnetic field B_{max}. Reversible processes are characterized by the fact that the resistance curve for increasing fields coincide with the curve for decreasing fields. This behavior can be identified for the topmost resistance curve in Fig. 8 with a maximum field of

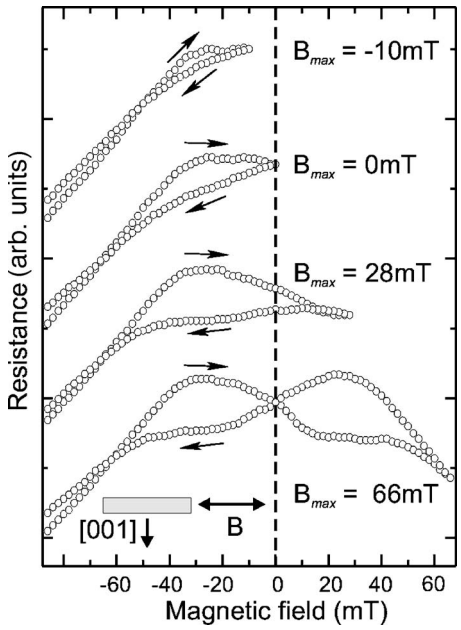

FIG. 8. Minor hysteresis loops measured at 4.2 K with increasing magnetic field amplitude (B_{max}) on the 2 μm wide *hard structure* with the magnetic field applied perpendicular to the [001] direction of CrO_2.

B_{max}=−10 mT. The three lower resistance curves exhibit different minor loops which demonstrate that the magnetization reversal process of these *hard structures* becomes irreversible at about 0 mT.

IV. CONCLUSION

In conclusion, a detailed study of magnetization configurations and magnetization reversal processes of microstructured epitaxial CrO_2 wires has been performed by means of MFM and magnetotransport measurements. Epitaxial CrO_2 wires of different widths have been prepared oriented along different crystallographic directions of the CrO_2(100) thin films: (i) with the wire long axis parallel to the [001] direction (the magnetic easy axis) and (ii) with the long axis perpendicular to the easy magnetic axis. For both geometries, the remanent micromagnetic structure was determined by means of MFM measurements showing the formation of a monodomain state in the case of the easy structure whereas for the hard structure the stripe domain configuration was observed. The temperature dependent MR measurements on both easy and hard structures show that at low temperatures the MR effects can be attributed to the ITMR effect between the CrO_2 crystallites and at higher temperatures to the AMR effect. MR measurements for different orientations of the CrO_2 wires to the external magnetic field and to the magnetocrystalline anisotropy directions showed that the magnetization reversal process of epitaxial CrO_2 wires are very sensitive to the interplay between the magnetocrystalline anisotropy, the shape anisotropy, and the Zeeman energy of the magnetic moments due to the applied field. The MR curve of a CrO_2 wire with its magnetocrystalline anisotropy acting perpendicular to the sum of the shape anisotropy and the external field cannot be explained without considering the CrO_2 film consisting of various crystallites each with microscopic magnetic easy axes that are slightly tilted with respect to the macroscopic easy axis of the continuous CrO_2 film.

ACKNOWLEDGMENT

The authors acknowledge support by the DFG through Grant No. SFB 513.

[1] M. N. Baibich, J. M. Broto, A. Fert, F. Nguyen Van Dau, F. Petroff, P. Etienne, G. Creuzet, A. Friederich, and J. Chazelas, Phys. Rev. Lett. **61**, 2472 (1988).

[2] G. Binasch, P. Grünberg, F. Saurenbach, and W. Zinn, Phys. Rev. B **39**, 4828 (1989).

[3] W. J. Gallagher, S. S. P. Parkin, Y. Lu, X. P. Bian, A. Marley, K. P. Roche, S. A. Rishton, C. Jahnes, T. M. Shaw, and G. Xiao, J. Appl. Phys. **81**, 3741 (1997).

[4] J. M. Daughton, J. Appl. Phys. **81**, 3758 (1997).

[5] H. Boeve, R. J. M. van der Veerdonk, B. Dutta, J. de Boeck, J. S. Moodera, and G. Borghs, J. Appl. Phys. **83**, 6700 (1998).

[6] X. W. Li, A. Gupta, and G. Xiao, Appl. Phys. Lett. **75**, 713 (1999).

[7] K. Schwarz, J. Phys. F: Met. Phys. **16**, L211 (1986).

[8] S. P. Lewis, P. B. Allen, and T. Sasaki, Phys. Rev. B **55**, 10253 (1997).

[9] M. A. Korotin, V. I. Anisimov, D. I. Khomskii, and G. A. Sawatzky, Phys. Rev. Lett. **80**, 4305 (1998).

[10] R. J. Soulen, Jr., J. M. Byers, M. S. Osofsky, B. Nadgorny, T. Ambrose, S. F. Cheng, P. R. Broussard, C. T. Tanaka, J. Nowak, J. S. Moodera, A. Barry, and J. M. D. Coey, Science **282**, 85 (1998).

[11] W. J. DeSisto, P. R. Broussard, T. F. Ambrose, B. E. Nadgorny, and M. S. Osofsky, Appl. Phys. Lett. **76**, 3789 (2000).

[12] Y. Ji, G. J. Strijkers, F. Y. Yang, C. L. Chien, J. M. Byers, A. Anguelouch, Gang Xiao, and A. Gupta, Phys. Rev. Lett. **86**, 5585 (2001).

[13] J. S. Parker, S. M. Watts, P. G. Ivanov, and P. Xiong, Phys. Rev. Lett. **88**, 196601 (2002).

[14] K. P. Kämper, W. Schmitt, G. Güntherodt, R. J. Gambino, and R. Ruf, Phys. Rev. Lett. **59**, 2788 (1987).

[15] Yu. S. Dedkov, M. Fonin, C. König, U. Rüdiger, S. Senz, D. Hesse, and G. Güntherodt, Appl. Phys. Lett. **80**, 4181 (2002).

[16] D. S. Rodbell, J. M. Lommel, and R. C. deVries, J. Phys. Soc. Jpn. **21**, 2430 (1966).

[17] A. Gupta, X. W. Li, and Gang Xiao, J. Appl. Phys. **87**, 6073 (2000).

[18] A. Toropova, G. Kotliar, S. Y. Savrasov, and V. S. Oudovenko, Phys. Rev. B **71**, 172403 (2005).

[19] L. Spinu, H. Srikanth, A. Gupta, X. W. Li, and Gang Xiao, Phys.

Rev. B **62**, 8931 (2000).
[20] F. Y. Yang, C. L. Chien, E. F. Ferrari, X. W. Li, G. Xiao, and A. Gupta, Appl. Phys. Lett. **77**, 286 (2000).
[21] G. Miao, G. Xiao, and A. Gupta, Phys. Rev. B **71**, 094418 (2005).
[22] J. M. D. Coey, A. E. Berkowitz, Ll. Balcells, F. F. Putris, and A. Barry, Phys. Rev. Lett. **80**, 3815 (1998).
[23] S. S. Manoharan, D. Elefant, G. Reiss, and J. B. Goodenough, Appl. Phys. Lett. **72**, 984 (1998).
[24] H. Y. Hwang and S.-W. Cheong, Science **278**, 1607 (1997).
[25] L. Ranno, A. Barry, and J. M. D. Coey, J. Appl. Phys. **81**, 5774 (1997).
[26] K. Suzuki and P. M. Tedrow, Phys. Rev. B **58**, 11597 (1998).
[27] K. Suzuki and P. M. Tedrow, Appl. Phys. Lett. **74**, 428 (1999).
[28] S. M. Watts, S. Wirth, S. von Molnár, A. Barry, and J. M. D. Coey, Phys. Rev. B **61**, 9621 (2002).
[29] X. W. Li, A. Gupta, T. R. McGuire, P. R. Duncombe, and G. Xiao, J. Appl. Phys. **85**, 5585 (1999).
[30] U. Rüdiger, M. Rabe, K. Samm, B. Özyilmaz, J. Pommer, M. Fraune, G. Güntherodt, S. Senz, and D. Hesse, J. Appl. Phys. **89**, 7699 (2001).
[31] M. Rabe, J. Pommer, K. Samm, B. Özyilmaz, C. König, M. Fraune, U. Rüdiger, G. Güntherodt, S. Senz, and D. Hesse, J. Phys.: Condens. Matter **14**, 7 (2002).
[32] F. Schwerer and J. Silox, Phys. Rev. Lett. **20**, 101 (1968).
[33] F. Schwerer and J. Silox, J. Appl. Phys. **39**, 2047 (1968).
[34] L. Berger, J. Appl. Phys. **55**, 1954 (1984).
[35] A. Yamaguchi, S. Nasu, H. Tanigawa, T. Ono, K. Miyake, K. Mibu, and T. Shinjo, Appl. Phys. Lett. **86**, 012511 (2005).
[36] M. Kläui, C. A. F. Vaz, J. A. C. Bland, W. Wernsdorfer, G. Faini, E. Cambril, L. J. Heyderman, F. Nolting, and U. Rüdiger, Phys. Rev. Lett. **94**, 106601 (2005).
[37] S. S. P. Parkin, U.S. Patent No. 6,834,005 (2004).
[38] M. Fonin, Yu. S. Dedkov, C. König, G. Güntherodt, U. Rüdiger, J. Mayer, D. Vyalikh, and S. Molodtsov, Adv. Solid State Phys. **43**, 487 (2003).
[39] A. Hubert and R. Schäfer, *Magnetic Domains* (Springer, New York, 1998).
[40] C. Kittel, Phys. Rev. **70**, 965 (1946).